Highly Toughened Polylactide with Novel Sliding Graft Copolymer by in Situ Reactive Compatibilization, Crosslinking and Chain Extension

Xue Li [a], Hailan Kang [a], Jianxiang Shen [a], Liqun Zhang [a, b *], Toshio Nishi [c], Kohzo Ito [d *], Changming Zhao [d] and Phil Coates [e]

[a] State Key Laboratory for Organic-Inorganic Composites, Beijing University of Chemical Technology, Beijing 100029, China

[b] Key Laboratory of Beijing City for Preparation and Processing of Novel Polymer Materials, Beijing University of Chemical Technology, Beijing 100029, China

[c] Department of Applied Physics, The University of Tokyo, Hongo, Bunkyo-ku, Tokyo 113, Japan

[d] Department of Advanced Materials Science, Graduate School of Frontier Sciences, The University of Tokyo, 5-1-5 Kashiwanoha, Kashiwa, Chiba 277-8561, Japan

[e] School of Engineering, Design and Technology, Bradford University, Bradford, BD7 1DP, UK

Abstract: The "sliding graft copolymer" (SGC), in which many linear poly-ε-caprolactone (PCL) side chains are bound to cyclodextrin rings of a polyrotaxane (PR), was prepared and employed to toughen brittle polylactide (PLA) with methylene diphenyl diisocyanate (MDI) by reactive blending. The SGC was in situ crosslinked and therefore transformed from a crystallized plastic into a totally amorphous elastomer during reactive blending. Meanwhile, PLA-*co*-SGC copolymer was formed at interface to greatly improve the compatibility between PLA and SGC, and the chain extension of PLA also occurred, were confirmed by FTIR, GPC, SEM, and TEM. The resulting PLA/SGC/MDI blends displayed super impact toughness, elongation at break and nice biocompatibility. It was inferred from these results the

crosslinked SGC (c-SGC) elastomeric particles with sliding crosslinking points performed as stress concentrators and absorbed considerable energy under impact and tension process.

KEYWORDS: polylactide, toughening, reactive compatibilization, sliding graft copolymer

1. Introduction

Polylactide (PLA) is a typical biodegradable polymer with excellent transparency, high strength and modulus, all of which make it suitable for use in various of fields, such as packaging, automotive industry and medical applications.[1] However, some inherent properties such as low flexibility and low impact strength limited its wider applications.[2, 3] Blending this brittle polymer with other biodegradable flexible polymers was considered to be a practical and useful way[4, 5] For example, blending PLA with various biodegradable polymers such as poly (ε-caprolactone) (PCL),[6, 7] poly (butylene succinate) (PBS),[8, 9] polyhydroxy butyrate (PHB),[10] starch,[11] and cellulose[12] can obtain new fully biodegradable PLA blends. However, some blends prepared by simple blending suffer from lower fracture properties due to the serious phase separation and poor interfacial adhesion between the two immiscible components[13]. An effective approach to solve the problem of poor compatibility of polymer blends is to use the reactive blending method[14-17]. Ray et al. used triphenyl phosphite (TPP) as the coupling agents in the reactive compatibilization of PLA and poly (butylene succinate-*co*-adipate) (PBSA). The impact strength and the elongation at break of PLA increased from 6 kJ/m^2 to 16 kJ/m^2, and 6% to 37% for

PLA/PBSA-TPP blend, respectively.[18] Oyama prepared super-tough PLA materials by reactive blending with poly (ethylene-glycidyl methacrylate) (EGMA). The elongation at break and the Izod impact strength increased by 9 times (35%) and by 15 times respectively compared with those of the neat PLA.[19] Therefore, in situ reactive blending method is a preferred technology for blending PLA with various polymers to improve its toughness.

It is well known that utilizing elastomers as tougheners to toughen brittle thermoplastic materials is a main and effective way. To achieve a good dispersion of the elastomer phase, most researchers and plastic enterprises tended to employ uncrosslinked elastomers to toughen the plastics because crosslinked elastomers could not be well dispersed in the plastic matrix by general melt blending technology. However, if the elastomer phase was crosslinked, the modulus and cohesive energy of elastomer phase could be improved for better comprehensive performance of the toughened blends. In recent years, ultrafine full-vulcanized powdered rubber (UFPR) as a new type of toughening modifier for polymer matrix has attracted much attention. As reported in many articles, UFPR can be directly blended into plastics as an effective toughening modifier for various polymer matrix such as epoxy,[20] polypropylene (PP),[21] poly(vinyl chloride) (PVC),[22] nlon-6,[23] etc. Ning et al. used ultrafine full-vulcanized powdered ethyl acrylate rubber (EA-UFPR) as the toughening modifier for PLA, resulting in a nice improvement in impact strength.[24] Zhang et al. had previously improved the impact strength of PLA by using a non-UFPR strategy. They considered a ternary blend system consisting of PLA, an

epoxy-containing elastomer (EBA-GMA), and a zinc ionomer (EMAA-Zn).[25] The zinc ions catalyzed the in situ crosslinking of the epoxy-containing elastomer and also promoted the reactive compatibilization at the interface of PLA and the elastomer, resulting in the excellent impact strength of PLA.

Recently, K. Ito' group prepared a novel type of polyrotaxane (PR) having polymeric side chains attached to the cyclic molecules, and designated it as "sliding graft copolymer" (SGC).[26, 27] The SGC, in which many linear poly-ε-caprolactone (PCL) side chains are bound to the cyclodextrin (α-CD) rings of a PR, were synthesized by ring-opening polymerization of ε-caprolactone initiated by the hydroxyl groups of PR (Scheme 1a). The bulky adamantine groups at both ends of the linear chains are introduced to prevent the dissociation of the cyclic molecules. The key feature of SGC is that the cyclic molecules (α-CD) and grafted side chains can freely slide and/or rotate along the backbone (PEG) within the restrictions of the main chain length. More interestingly, crosslinking the side chains (PCL) of SGC can produce a novel three-dimensional supramolecular network. When the crosslinked SGC (c-SGC) undergoes considerable swelling or elongation, the crosslinks can slide on the included PEG chains to their optimum points, resulting in full tension of all polymer chains and relaxation of internal stresses.[28, 29] This phenomenon, which is called the pulley effect, is illustrated in Scheme 1(c). What's more, the chemical contituents of SGC, i.e., PCL, PEG and α-CD (Scheme 1(c)) are biodegradable and part of them can be derived from renewable resources, giving SGC biodegradable and biocompatible characteristics.

Considering the special mechanical performance and biodegradable nature of SGC, we for the first time try to use the novel SGC to toughen PLA through reactive blending with the assistance of MDI. The morphology, thermal and crystallization behaviors, and mechanical properties of the blends are systematically investigated. Such a novel PLA blend with super toughness was not reported before.

2. Experimental section

2.1. Materials

Polylactide (PLA, 2002D) was provided by Natureworks, USA. It had a weight-average molecular weight (M_w) of ~167, 000 g/mol, a polydispersity index (*PDI*) of 1.52 (obtained by GPC), and a glass transition temperature and melting point of 60 ^{o}C and 155 ^{o}C (obtained by DSC), respectively. The chemical structure of SGC is shown in Scheme 1(b). The SGC was prepared by the so-called ‘‘bulk polymerization’’ of ε-CL monomers, which was initiated by the hydroxyl groups of the hydroxypropylated CDs and catalyzed by tin 2-ethylhexanoate (stannous octoate, $Sn(Oct)_2$). In this method, ε-CL (10 ml) and hydroxypropylated polyrotaxane (1 g) were added into a 50-ml three-neck flask. The mixture was purged with nitrogen for 30 min under gentle magnetic stirring until the mixture was uniform. In the second phase, after adding $Sn(Oct)_2$ as the catalyst, the mixture was heated to 100 ^{o}C under an argon atmosphere for 3~4 h until the liquid became viscous. Then the liquid was dissolved in toluene (40 ml) and poured into hexane (450 ml) to precipitate the SGC. The resulting SGC was obtained after removing the remaining liquids in vacuo. The SGC (M_w ~ 852, 000 g/mol, as obtained from GPC) contained PEG (M_w ~ 35,000),

α-CD (Mw ~ 1000).With about 103 α-CDs per molecule, the SGC has an inclusion ratio of 26%. The synthesis technology of this kind of SGC with the CAS Number of 928045-45-8 JPN has been commercialized, and the SGC can be purchased from Tianjing MicroRheo Supermolecular Materials LLC. More detailed information about SGC can be found in our previous work.[26] MDI was provided by Yantai Wanhua Polyurethanes Infine Co. Ltd.

2.2. Samples Preparation

PLA and SGC were dried in a vacuum oven at 60 ^{o}C for at least 24 h before processing. Firstly, PLA was pre-melted by Haake mixer (Rheomix 600p, Thermal Electron Co., USA) in a conventional melt-mixer at 170 ^{o}C and a rotor speed of 20 rpm for 2 min and then increased to 80 rpm. Then the SGC was added into the internal mixer for 3 min. Subsequently, the MDI with different concentrations was added into the PLA/SGC blend in Haake mixer at 170 ^{o}C, 80 rpm for 7 min. The total blending time after the samples were placed in the mixing chamber was 12 min. And neat PLA and PLA/MDI (50/2) blend were prepared under the same experimental conditions. All the samples were finally hot-pressed into 1-mm thick sheets under 10 MPa at 190 ^{o}C for 5 min.

2.3. Characterization

Scanning electron microscopy (SEM) (S4700, Hitachi Co., Japan) was used to determine the morphologies of the blends at 1 kV. The samples were fractured under cryogenic conditions for 10 min and the surfaces were coated with a thin gold layer.

The average molecular weight and polydispersity index of all the samples were

determined by gel permeation chromatography (GPC) measurements on a Waters Breeze instrument equipped with three water columns (Steerage HT3 HT5 HT6E) using tetrahydrofuran as the eluent (1 ml/min) and a Waters 2410 refractive index detector. A polystyrene standard was used for calibration.

Fourier transform infrared (FTIR) spectra were recorded on a Tensor 27 spectrometer. Typically, 32 scans at a resolution of 4 cm^{-1} were accumulated to obtain one spectrum.

Differential scanning calorimetry (DSC) data were obtained from a Mettler-Toledo DSC instrument under nitrogen, using samples of approximately 6-8 mg. All samples were heated to 200 ^{o}C at 50 ^{o}C/ min and kept for 5 min to remove any previous thermal history. Then they were cooled to -100 ^{o}C at 10 ^{o}C /min, and reheated up to 200 ^{o}C at 10 ^{o}C /min to determine the glass transition temperature (T_g), cold crystallization temperature (T_c) and melting temperature (T_m).

X-ray diffractograms (XRD) were obtained at room temperature on a Rigaku RINT 2000 instrument, using Ni-filtered Cu Kα radiation (40 kV, 100 mA). Data were obtained from 2θ=10-36^{o} at a scanning rate of 3.35 ^{o}/min.

Transmission electron microscopy (TEM) was performed on H-800-1 transmission electron microscope (Hitachi Co., Japan) at 200 kV. Ultrathin film (<100 nm thickness) specimens were obtained by using a diamond blade on a RMC microtome station. For TEM observations, the samples were stained with ruthenium tetroxide (RuO_4) for 20 min.

Type-V dumbbell-shaped specimens were molded dimensions of approximately

62×1 mm (L×T) and tested at room temperature according to ASTM D638 by using a CMT 4104 Electrical Tensile Instrument (Shenzhen SANS Test Machine Co., Ltd. China) at 5 mm/min. The impact test specimens were molded with dimensions of approximately 80×10×4mm (L×W×T), and measured by using a Ceast Resil Impactor according to ISO180-2000. Specimens were notched on one side, with a depth of around 0.2 mm using a Ceast notcher. At least five specimens were tested for an average value.

3. Results and Discussion

3.1 SEM morphology of PLA/SGC/MDI blends.

If the dispersion phase is incompatible with the matrix phase, the dispersion would exist as spherical particles with large dimension to reduce surface tension. On the contrary, if the two components in a binary blend have good compatibility, the dispersion particles would uniformly disperse in the matrix with relatively smaller particle size and has no obvious demarcation with matrix phase.[30-33] The SEM of cryo-fractured surfaces of PLA/SGC (40/10) and PLA/SGC/MDI blends with different amounts of MDI are employed to study the phase morphology, as shown in Figure 1. The PLA/SGC (40/10) blend (Figure 1(a) and (a1)) presents distinct two-phase island-sea type morphologies. The spherical structures are the dispersed SGC phases. The compatibility between PLA and SGC is poor as evidenced by the obvious interface voids between the SGC particles and the PLA matrix. However, after the addition of MDI, the spherical structures and the interface cracks of PLA/SGC/MDI blends gradually disappear. In addition, the torque of the

PLA/SGC/MDI blend rises rapidly after the addition of MDI (see Figure S1 in the Supporting Information). In other words, the melt viscosity of the PLA/SGC/MDI blend increased during processing. The increase in viscosity could contribute to the morphology modification by preventing SGC aggregation. But the principal cause for the improvement of compatibility has been attributed to the in situ formation of PLA-*co*-SGC copolymer at the interface of two immiscible polymers. The in situ reaction between the isocyanate group of MDI and hydroxyl groups of PLA and side chain PCL resulted in PLA-*co*-SGC copolymers containing carbamate linkages. And this in situ compatibilization will be further discussed in the following analysis.

3.2 In situ reaction between PLA and MDI

The PLA/MDI (40/2) blend was prepared to determine the reaction between PLA and MDI. GPC traces were used to monitor the change of M_w from PLA to PLA/MDI blend, as shown in Figure 2(a). The GPC chromatogram of the neat PLA contained a single peak. For the PLA/MDI (50/2) blend, the major peak is found at lower elution time than neat PLA, and the broad shoulder peak is assigned to the chain extended polymer. M_w of PLA/MDI blend is 329,000, which is almost double that of the neat PLA (M_w ~167,000). Meanwhile, the *PDI* also increases from 1.52 for PLA to 2.52 for PLA/MDI, owing to the chain extension of PLA induced by MDI. It was suggested that isocyanate group (-N=C=O) of MDI can connect the hydroxyl end groups (-OH) of PLA molecules through carbamate bonds so as to double the M_w and *PDI*, and the reaction of chain extension is shown in Scheme 2(a). The reaction of chain extension can be further confirmed by FTIR, as shown in Figure

2(b). For the PLA/MDI blend, a typical absorbance from carbamate (—NH—C(=O)—O—) appeared at approximately 1545, 1636 and 3305 cm^{-1}. The new stretch at 1636 cm^{-1} can be assigned to an amide carbonyl-stretching mode (υ(C=O)), which is so-called Amide I vibrational stretch. The new band at 1545 cm^{-1} corresponds to the coupling of the N-H stretching vibration (υ(N=H)) with the N-H deformation vibration (δ(N-H)), which is so-called Amide II vibration.[34] And the new stretch at 3305 cm^{-1} has been assigned to the free vibration of N-H stretching mode in carbamate units. As a consequence, MDI is proven to be an effective chain extender to produce high molecular weight PLA. Higher molecular weights are better for PLA to possess good physical properties.

3.3 In situ crosslinking of SGC and formation of PLA-co-SGC

To determine the in situ crosslinking of SGC and formation of PLA-*co*-SGC with MDI, neat PLA, PLA/MDI (50/2), PLA/SGC (40/10), and PLA/SGC/MDI (40/10/2) blends were firstly dissolved in trichloromethane and the photographs of these solution appearance are shown in Figure S2 in the Supporting Information. By visual observations, all the solutions were clear except that of the PLA/SGC/MDI (40/10/2) blend which is turbid. The trichloromethane is a good solvent for PLA as reported. The insoluble substance is believed to be the reaction product of MDI, SGC and PLA, is expected to form a crosslinked network. Secondly, the solvent extraction technique was employed to determine the insoluble component in the PLA/SGC/MDI blend. The PLA/SGC/MDI blend was extracted for 72h at 150°C in trichloromethane solvent, and then dried for solution removal. The insoluble component was characterized with

FTIR and DSC, as shown in Figure 3 and Figure 4. In order to confirm the crosslinking of SGC with MDI more explicitly and conveniently, the SGC/MDI blend was placed in a flask in the absence of PLA and allowed to react for 10 min at 170°C. When MDI were poured into the melting SGC, the gelation and solid mass were generated immediately. The resultant formed in flask was also analyzed by FTIR and DSC.

A detailed FTIR analysis of pure SGC, SGC/MDI particles (c-SGC formed in flask) and extracted insoluble fraction (extracted c-SGC) were conducted in order to prove the relative reactions, and the spectra are shown in Figure 3. For the pure SGC, the most striking absorption peak in the spectrum appears at 1730 cm^{-1}, which is attributed to the carbonyl stretching in the PCL side chains [35]. Besides, the bands at 2941, 2865, 1294, and 1240 cm^{-1} are assigned to the asymmetric CH_2 stretching ($\upsilon_{as}(CH_2)$), symmetric CH_2 stretching ($\upsilon_{s}(CH_2)$), C-C and C-O stretching modes in the crystalline PCL (υ_{cr}) and asymmetric COC stretching ($\upsilon_{as}(COC)$), respectively.[35] A comparison with the spectra of pure SGC and c-S**G**C (formed in flask), new absorption peaks appeared at 1530, 1620, and 3320 cm^{-1} in the spectrum of c-SGC (as shown in the top right of Figure 4) are the characteristic carbamate absorption peaks. Besides, the absorbance peak of -OH at 3500 cm^{-1} in the spectrum of pure SGC almost disappears, because the hydroxyl groups are consumed by the crosslinking reaction (as shown in the top left of Figure 4). These peaks accounted for the crosslinking reaction of SGC induced by MDI. Similarly, for the extracted c-SGC, the characteristic carbamate bands are also observed. Moreover, stretching vibration CH_3

($\upsilon(CH_3)$) and deformation vibration of CH_3 ($\delta(CH_3)$) of PLA molecules located at 2910 and 1413 cm^{-1} respectively [36] were also observed, which suggested the existence of PLA component in the extracted c-SGC insoluble substance in PLA/SGC/MDI (40/10/2) (as shown in the bottom left and right of Figure 3) . Thus, we can conclude that very active -N=C=O group can connect the -OH of PLA and side chains PCL of SGC to form the PLA-*co*-SGC copolymer. A schematic illustration of the PLA-*co*-SGC is shown in Scheme 2(b). The PLA-*co*-SGC copolymer can reduce the interfacial tension and increase the interfacial adhesion, thus acting as a compatibilizer. Furthermore, the network of c-SGC might physically interlock with the PLA chains to reduce the phase separation of SGC from the PLA phase. DMTA will further confirm the molecular interaction of PLA with SGC and c-SGC in section 3.5.

The DSC curves of pure SGC, c-SGC particles (formed in the flask), and the extracted c-SGC are shown in Figure 4. The pure SGC shows two transition peaks upon heating: a T_g at around -50.3^{o}C and a T_m at 33.8^{o}C, which illustrates that SGC is a semi-crystallined plastic resin even though its T_g is much lower than room temperature. However, this melting peak disappears in the thermographs of the c-SGC particles formed in the flask and the extracted c-SGC, an indication that SGC is completely transformed into amorphous elastomer. Besides, the T_g shifts from -50.3°C for pure SGC to -45.8°C for c-SGC formed in the flask because of the restriction of the segmental mobility of SGC molecular chains by crosslinking. A further restriction due to the comparatively rigid PLA molecules existing in extracted c-SGC, causes the shift of T_g to higher temperature (-40.1°C) compared with the one formed in flask

(-45.8°C). In a summary, it is concluded that the amorphous elastomer particles were prepared by in situ crosslinking of SGC with MDI in the PLA matrix. At the same time the PLA-*co*-SGC copolymer formed in the interface can act as compatibilizer to improve the compatibility between PLA and SGC phase. It is expected that the crosslinked amorphous elastomeric particles can act as stress concentrators to absorb more fracture energy for toughening of PLA and other plastics.

3.4. Morphology of SGC and c-SGC in PLA matrix

TEM was employed to evaluate the morphology and dispersion of pure SGC and c-SGC particles in the PLA matrix. In Figure 5, SGC was observed as the dark phase in the TEM micrographs. The TEM image of the PLA/SGC (40/10) blend reveals the sea-island morphology (Figure 5(a), (a1)). The SGC domains are clearly dispersed in the PLA matrix and exist as dark spheres with regular shapes due to the weak interfacial interaction. After the addition of MDI, the shape of the c-SGC particles (dark phase) become more irregular. During reactive mixing the in situ crosslinking of SGC and the in situ formation of PLA-co-SGC occurred; thus, both the cohesive energy of the SGC phase and the interfacial interaction between SGC phase and PLA phase were apparently increased. However, the in situ reactions and the dispersion process of SGC are complicated partly because the dispersion and diffusion of MDI molecules in SGC phase and PLA phase is complex during reactive blending. The size distribution of SGC and c-SGC particles are summarized in Figure S3 in the Supporting Information. It can be clearly observed that the size dispersion of c-SGC particles is broader than that of SGC in PLA matrix. The complex reactions,

dispersion and fragmentation process of the SGC phase lead to a broad size distribution and heterogeneous morphology.

3.5 Dynamical mechanical thermal analysis.

DMTA was employed to investigate the molecular interaction of PLA with SGC and c-SGC. The plots of loss factor (tan δ) versus temperature for the neat PLA, PLA/SGC (40/10) blend, and PLA/SGC/MDI blends with different amounts of MDI are shown in Figure 6. For the PLA/SGC (40/10) blend, there are two peaks at -44^{o}C and 65^{o}C, corresponding to the T_g of SGC and PLA, respectively.[37] The T_g (65^{o}C) of PLA in the PLA/SGC blend is slightly lower than that of the neat PLA (67^{o}C), an indication that there is some molecular interaction between PLA and SGC, but this interaction is not strong because of the distinct difference of molecular structure of two polymer and phase separation. On the other hand, all the PLA/SGC/MDI blends demonstrate two T_gs, corresponding to the T_g of c-SGC and that of PLA. The T_g of c-SGC shifts to higher temperatures with increasing amount of MDI. The T_g of c-SGC in PLA/SGC/MDI (40/10/2) is 18^{o}C higher than that in PLA/SGC (40/10), in line with the DSC results mentioned above. What is more, T_g of PLA shifts to lower temperatures with increasing MDI concentration due to the increase of interfacial interaction. The T_g of c-SGC and the T_g of PLA in the PLA/SGC/MDI blend shift towards each other, an indication of improved compatibility between PLA and SGC through reactive compatibilization. Besides, the peak at around 105 ^{o}C is assigned to the cold crystallization of PLA. Cold crystallization refers to a phenomenon that some glassy polymers, after heated to temperatures higher than T_g, are able to crystallize.

The effect of SGC and c-SGC on the cold crystallization of PLA will be further discussed in the DSC analysis.

3.6 Thermal behavior and crystallization

Figure 7(a) shows the DSC heating curves of neat PLA, PLA/SGC and PLA/SGC/MDI blends with different amounts of MDI, and the data are summarized in Table 1. The neat PLA curve shows three transitions upon heating: a PLA glass transition, a broad cold crystallization exothermic peak, and a melting endothermic peak. The low and broad cold crystallization peak indicates that neat PLA has a rather low cold crystallization capability. However, after the addition of SGC into PLA, the cold crystallization peak shifts to lower temperature and the full width at half maximum becomes smaller than that of neat PLA, probably because SGC has a dilution effect on the PLA matrix, i.e., SGC is in a highly elastomeric state at the cold crystallization temperature of PLA since it is already melted. Therefore, SGC improves the mobility of PLA segment and the crystallization ability of PLA. However, the cold crystallization temperature increases with the addition of MDI indicating a decrease in cold crystallization ability of PLA. There are three likely reasons for this phenomenon: the increase of molecular weight of PLA due to chain extension; the in situ crosslinking of SGC, and the chemical bonding between PLA and c-SGC. The chemical bonding between PLA and c-SGC prevents the PLA molecules from stepping into the crystal lattice of PLA, so that it partly restrains the advantage of c-SGC by increasing the mobility of PLA molecules. Moreover, the curves for the PLA/SGC (40/10) and PLA/SGC/MDI (40/10/0.5) blends show an

additional melting exothermic peaks around 35°C, regarded as the T_m of SGC. The melting peak of SGC decreased gradually with increasing MDI content and completely disappears in PLA/SGC/MDI (40/10/1), indicating that SGC has finally transformed into an amorphous network when the crosslink reaction is complete.

The crystalline structure of pure SGC, neat PLA, PLA/SGC blend and PLA/SGC/MDI blends with different amounts of MDI are also investigated by XRD, and the patterns are shown in Figure 7(b). The pattern for SGC shows three strong diffraction peaks at 2θ=21.4, 22.0, and 23.8^o, corresponding to the (110), (111), and (200) planes, respectively, of the orthorhombic crystal form of the PCL side chains in SGC.[38] The broad diffraction peak for the neat PLA indicates that the PLA is amorphous or the amount of crystallites is too low to be traced.[39] The XRD patterns for the PLA/SGC and PLA/SGC/MDI (40/10/0.5) blends show typical but weak reflections of SGC, indicating that the crystalline structure of SGC remains the same in blends. The diffraction peaks completely disappear when the MDI content is 2 g per 100 g polymer or more, indicating that the crosslinked SGC already became amorphous, in good agreement with the DSC results. The transformation of SGC from semi-crystallized plastic into elastomer will be very beneficial to the high toughness of PLA blends.

3.7 Mechanical properties

The stress-strain curves of neat PLA, PLA/SGC blend and PLA/SGC/MDI blends with different amounts of MDI are presented in Figure 8 (a), with details listed in Table S1. PLA is very rigid and shows a high tensile strength, but its elongation at

break of about 13% indicates that it undergoes brittle fracture. The PLA/SGC blend is as brittle as neat PLA because the SGC maintains crystallized state in PLA/SGC blend rather than high elastic state at the room temperature. What's more, the PLA/SGC shows relatively low tensile strength because of low strength of SGC phase and very weak interface adhesion between PLA and SGC. But after the addition of MDI, the strength of the PLA/SGC/MDI blends increase gradually. And the elongation at break of the PLA/SGC/MDI (40/10/2) blend increase to 236%, nearly 18 times improvement than neat PLA, as clearly shown in Figure 9 (b). The PLA/SGC/MDI blend showed initial strain softening and visually considerable stress whitening after yielding and then underwent stable neck growth; a brittle-to-ductile transition occurred due to the presence of c-SGC particles. Because the c-SGC is a special elastomer with crosslinking points that can slide under the stress, and the interfacial interaction between c-SGC phase and PLA phase is stronger due to in situ compatibilization, thus the remarkable plastic deformation of PLA matrix can be brought by the presence of c-SGC particles. Tensile toughness-the area under the stress-strain curve of a given material-was a convenient measurement to demonstrate the ductility of the materials during low speed fracture process. The effect of MDI content in the blends on tensile toughness have been given in Figure 8(b). It can be seen that the tensile toughness of the PLA/SGC/MDI blends is significantly improved with the increase of MDI content. The tensile toughness of the PLA/SGC/MDI (40/10/2) blend increases to 79 MJ/m^3, nearly 20 times improvement than neat PLA.

Notched impact strength is a more accurate and more useful measurement to

evaluate the toughness than the tensile method due to the introduction of a sharp notch. Figure 9 shows the notched impact strength of neat PLA, PLA/SGC blend and PLA/SGC/MDI blends with different amounts of MDI. Although there is a slight increase of impact strength when SGC is added to PLA, a significant increase in toughness was only realized with the formation of c-SGC. The notched impact strength is further increased to about 48.6 kJ/m^2, which is about 20 times higher than that of neat PLA. Our results show that the formation of c-SGC particles with special sliding characteristics of crosslinks and the formation of excellent interfacial interaction by in situ compatibilization are very effective in overcoming the brittleness of PLA, resulting in significant improvements of mechanical properties. The improvements of mechanical properties surpass those by many previous efforts in toughening PLA (Table S2). Though some PLA blends displayed a significant increase in impact strength over that of neat PLA, most of the added polymers have no biocompatibility. The lack of biocompatibility limits the biomedical applications of the prepared blends. Our work provides an effective toughening method to largely improve the mechanical properties of PLA without sacrificing its biocompatibility (Figure S4 in the Supporting Information), which is very important for the wide application of PLA materials.

3.8 Morphology of fracture surface

We further investigate the toughening effect of SGC on PLA by using SEM, and the SEM micrographs of the tensile-fractured surfaces of neat PLA, PLA/SGC (40/10), and PLA/SGC/MDI (40/10/2) are presented in Figure 10. The tensile-fractured

surface of neat PLA is flat, indicating the neat PLA undergoes brittle fracture. However, the tensile-fractured surface of the PLA/SGC (40/10) blend is much rougher than that of neat PLA, with many small fibrils and cavities created by the removal of SGC particles. But there is no significant deformation of the PLA matrix. Since the interfacial adhesion between PLA and SGC is weak, relatively soft SGC particles first deform and are removed by tensile stress. On the other hand, the tensile-fractured surface of the PLA/SGC/MDI (40/10/2) blend exhibits highly elongated fibrils and a large degree of matrix deformation, indicating that a brittle-to-ductile transition occurs in the presence of c-SGC particles. Since c-SGC particles have much lower elastic modulus than the PLA matrix, these particles act as stress concentrators under tensile stress. More importantly, under external loading, the c-SGC particles have the advantage that the crosslinking points can slide along the linear chains to the optimum points (Scheme 1(c)). During tensile process, the c-SGC particles will effectively induce matrix shear yielding under the support of excellent interfacial interaction because the supramolecular network is extremely easy to deform and distribute the tensile stresses, thus preventing the early destruction of the blends.

Figure 11 shows the SEM micrographs of the impact-fractured surfaces of neat PLA, PLA/SGC (40/10) blend and PLA/SGC/MDI (40/10/2) blend. Similarly, the surface of neat PLA is smooth, an indication of the brittle failure of PLA under impact loading. The impact-fractured surface of PLA/SGC (40/10) shows inhomogeneity and many spherical voids, indications of interfacial debonding caused by the weak interfacial adhesion between PLA and SGC, and brittle failure. The impact-fractured

surface of the PLA/SGC/MDI (40/10/2) blend is very rough, with considerably orientated plastic deformation and many cavities possibly generated inside of the c-SGC particles along the impact direction. In a rubber-toughened plastic system, two kinds of cavitations can be formed under impact or tensile testing: (1) the internal cavitations within the cores of rubber particles when there is a strong interfacial adhesion between the components and relatively low strength of the rubber phase itself and (2) the debonding cavitations at the interfaces when the interfacial adhesion is not sufficiently high.[40] Because there is not sufficient interfacial adhesion between SGC and PLA, instead of cavitations within the SGC core under the triaxial stress, interfacial debonding took place. Thus, there is only a slight increase in toughness when SGC is added to PLA without MDI. For the PLA/SGC/MDI (40/10/2) blend, a strong interfacial adhesion between PLA and SGC is obtained by the in situ reactive compatibilization, the very soft c-SGC particles with slide crosslinking points acted as stress concentrators. During fast impact process, c-SGC particles will firstly induce matrix shear yielding mainly because this supramolecular network is very easy to deform and distribute the impact load, and then with the development of deformation, the c-SGC particles will generate cavitations due to the destruction of themselves. Both two processes will absorb considerable fracture energy under impact process.

4. Conclusion

In summary, polylactide (PLA) blends with very high toughness were successfully prepared by reactive melt blending with sliding graft copolymer (SGC) and reactive agent methylene diphenyl diisocyanate (MDI). The super toughening

effect of SGC in PLA mainly ascribed to the in situ generations of PLA-*co*-SGC copolymer and crosslinked SGC particles. Though PLA and SGC are incompatible, the in situ formation of PLA-*co*-SGC copolymer can act as effective compatibilizers to enhance the compatibility between two immiscible polymers. The presence of crosslinked SGC in the PLA matrix improved the notched Izod impact strength and elongation at break by 20 and 18 times respectively over those of unmodified PLA. These improved values are much higher than most values reported data in most literatures. All the experiments demonstrated that the crosslinked SGC particles with slide crosslinking points performed as stress concentrators could absorb more fracture energy under tensile and impact process. Besides, the in vitro cytotoxicity tests showed that these blends are nontoxic towards mouse fibroblasts, which could endow the resulting blend with a wide potential application in both engineering field and medical field. This methodology can also be utilized to toughen other brittle polymers such as epoxy resin, polyester plastics and polycarbonate by adjusting the molecular structures of SGC and interfacial agents.

Acknowledgements

This work was supported by the National Natural Science Foundation of China (50933001, 51221002 and 51320105012).

Captions of Schematics, Figures and Tables:

Scheme 1. (a) Schematic illustration of the preparation of a sliding graft copolymer (SGC), (b) structure schematic of SGC, (c) pulley effect.

Scheme 2. Synthesis scheme of (a) chain extension of PLA with MDI, (b) compatibilizer PLA-*co*-SGC.

Figure 1. SEM images of cryo-fractured surface of PLA/SGC/MDI blends (a)-(a1) 40/10/0, (b)-(b1) 40/10/0.5, (c)-(c1) 40/10/1, (d)-(d1) 40/10/2.

Figure 2. (a) GPC traces and (b) FTIR spectra of neat PLA and PLA/MDI (50/2) blend.

Figure 3. FTIR spectra of (A) neat PLA; (B) pure SGC; (C) c-SGC particles (extracted); (D) c-SGC particles (formed in flask).

Figure 4. DSC curves of (A) pure SGC; (B) c-SGC particles (formed in flask); (C) c-SGC particles (extracted).

Figure 5. Transmission electron micrographs of (a)-(a1) PLA/SGC (40/10), (b)-(b1) PLA/ SGC/MDI (40/10/0.5), (c)-(c1) PLA/ SGC/MDI (40/10/2).

Figure 6. Plots of loss factor (tan δ) against temperature for (a) neat PLA, (b) PLA/SGC (40/10), (c) PLA/SGC/MDI (40/10/0.5), (d) PLA/SGC/MDI (40/10/1), and (e) PLA/SGC/MDI (40/10/2).

Figure 7. (a) DSC thermograms (second heating) and (b) XRD patterns of neat PLA, pure SGC, PLA/SGC, and PLA/SGC/MDI with different MDI amounts.

Figure 8. (a) Stress- strain curves and (b) tensile toughness and strain at break of PLA/SGC and PLA/SGC/MDI with different MDI contents.

Figure 9. Notched impact strength of neat PLA, PLA/SGC, and PLA/SGC/MDI with different MDI contents.

Figure 10. SEM images of tensile-fractured surface of (a)-(a1) neat PLA, (b)-(b1) PLA/SGC (40/10) and (c)-(c1) PLA/SGC/MDI (40/10/2).

Figure 11. SEM images of impact-fractured surface of (a) neat PLA, (b)-(c) PLA/SGC (40/10), and (d)-(f) PLA/SGC/MDI (40/10/2).

Table 1. DSC parameters obtained from second heating scan of PLA and PLA/SGC/MDI blends

References

1. Drumright, R. E.; Gruber, P. R.; Henton, D. E. *Advanced Materials* **2000,** 12, (23), 1841-1846.
2. Chen, B. K.; Shen, C. H.; Chen, S. C.; Chen, A. F. *Polymer* **2010,** 51, (21), 4667-4672.
3. Kang, H.; Qiao, B.; Wang, R.; Wang, Z.; Zhang, L.; Ma, J.; Coates, P. *Polymer* **2013,** 54, (9), 2450-2458.
4. Madhavan Nampoothiri, K.; Nair, N. R.; John, R. P. *Bioresource Technology* **2010,** 101, (22), 8493-8501.
5. Jiang, L.; Wolcott, M. P.; Zhang, J. *Biomacromolecules* **2005,** 7, (1), 199-207.
6. Takayama, T.; Todo, M. *J Mater Sci* **2006,** 41, (15), 4989-4992.
7. Na, Y. H.; He, Y.; Shuai, X.; Kikkawa, Y.; Doi, Y.; Inoue, Y. *Biomacromolecules* **2002,** 3, (6), 1179-1186.
8. Shibata, M.; Inoue, Y.; Miyoshi, M. *Polymer* **2006,** 47, (10), 3557-3564.
9. Yokohara, T.; Yamaguchi, M. *European Polymer Journal* **2008,** 44, (3), 677-685.
10. Abdelwahab, M. A.; Flynn, A.; Chiou, B.-S.; Imam, S.; Orts, W.; Chiellini, E. *Polymer Degradation and Stability* **2012,** 97, (9), 1822-1828.
11. Zhang, J.-F.; Sun, X. *Biomacromolecules* **2004,** 5, (4), 1446-1451.
12. Huda, M. S.; Mohanty, A. K.; Drzal, L. T.; Schut, E.; Misra, M. *J Mater Sci* **2005,** 40, (16), 4221-4229.
13. Broz, M. E.; VanderHart, D. L.; Washburn, N. R. *Biomaterials* **2003,** 24, (23), 4181-4190.
14. Wang, L.; Ma, W.; Gross, R. A.; McCarthy, S. P. *Polymer Degradation and Stability* **1998,** 59, (1–3), 161-168.
15. Harada, M.; Iida, K.; Okamoto, K.; Hayashi, H.; Hirano, K. *Polymer Engineering & Science* **2008,** 48, (7), 1359-1368.
16. Xanthos, M.; Dagli, S. S. *Polymer Engineering & Science* **1991,** 31, (13), 929-935.
17. Ding, Y.; Xin, Z.; Gao, Y.; Xu, X.; Yin, J.; Costa, G.; Falqui, L.; Valenti, B. *Macromolecular Materials and Engineering* **2003,** 288, (5), 446-454.
18. Ojijo, V.; Sinha Ray, S.; Sadiku, R. *ACS Applied Materials & Interfaces* **2013,** 5, (10), 4266-4276.
19. Oyama, H. T. *Polymer* **2009,** 50, (3), 747-751.
20. Huang, F.; Liu, Y.; Zhang, X.; Wei, G.; Gao, J.; Song, Z.; Zhang, M.; Qiao, J. *Macromolecular Rapid Communications* **2002,** 23, (13), 786-790.
21. Liu, Y.; Zhang, X.; Gao, J.; Huang, F.; Tan, B.; Wei, G.; Qiao, J. *Polymer* **2004,** 45, (1), 275-286.
22. Wang, Q.; Zhang, X.; Dong, W.; Gui, H.; Gao, J.; Lai, J.; Liu, Y.; Huang, F.; Song, Z.; Qiao, J. *Materials Letters* **2007,** 61, (4–5), 1174-1177.
23. Dong, W. F.; Liu, Y. Q.; Zhang, X. H.; Gao, J. M.; Huang, F.; Song, Z. H.; Tan, B. H.; Qiao, J. L. *Macromolecules* **2005,** 38, (11), 4551-4553.
24. Zhao, Q.; Ding, Y.; Yang, B.; Ning, N.; Fu, Q. *Polymer Testing* **2013,** 32, (2), 299-305.
25. Liu, H.; Song, W.; Chen, F.; Guo, L.; Zhang, J. *Macromolecules* **2011,** 44, (6), 1513-1522.
26. Araki, J.; Kataoka, T.; Ito, K. *Soft Matter* **2008,** 4, (2), 245-249.
27. Araki, J.; Ito, K. *Soft Matter* **2007,** 3, (12), 1456-1473.
28. Karino, T.; Okumura, Y.; Ito, K.; Shibayama, M. *Macromolecules* **2004,** 37, (16), 6177-6182.
29. Kato, K.; Ito, K. *Reactive and Functional Polymers* **2013,** 73, (2), 405-412.
30. Porter, R. S.; Wang, L.-H. *Polymer* **1992,** 33, (10), 2019-2030.
31. Ma, J.; Feng, Y. X.; Xu, J.; Xiong, M. L.; Zhu, Y. J.; Zhang, L. Q. *Polymer* **2002,** 43, (3), 937-945.

32. Martin, P.; Devaux, J.; Legras, R.; van Gurp, M.; van Duin, M. *Polymer* **2001,** 42, (6), 2463-2478.
33. Legros, A.; Carreau, P. J.; Favis, B. D.; Michel, A. *Polymer* **1994,** 35, (4), 758-764.
34. Stankovich, S.; Piner, R. D.; Nguyen, S. T.; Ruoff, R. S. *Carbon* **2006,** 44, (15), 3342-3347.
35. Elzein, T.; Nasser-Eddine, M.; Delaite, C.; Bistac, S.; Dumas, P. *Journal of Colloid and Interface Science* **2004,** 273, (2), 381-387.
36. Krikorian, V.; Pochan, D. J. *Macromolecules* **2005,** 38, (15), 6520-6527.
37. Sinha Ray, S.; Maiti, P.; Okamoto, M.; Yamada, K.; Ueda, K. *Macromolecules* **2002,** 35, (8), 3104-3110.
38. Chen, E.-C.; Wu, T.-M. *Polymer Degradation and Stability* **2007,** 92, (6), 1009-1015.
39. Wang, R.; Wang, S.; Zhang, Y.; Wan, C.; Ma, P. *Polymer Engineering & Science* **2009,** 49, (1), 26-33.
40. Pearson, R. A.; Yee, A. F. *J Mater Sci* **1991,** 26, (14), 3828-3844.

Table 1. DSC parameters obtained from second heating scan of PLA and PLA/SGC/MDI blends

PLA/SGC/MDI	SGC	PLA					
	T_m (℃)	T_g(℃)	T_c(℃)	$\triangle H_c$(J/g)	T_{m1}(℃)	T_{m2}(℃)	$\triangle H_m$ (J/g)
50/0/0	-	60.0	126.3	-	-	155.1	2.38
40/10/0	36.8	59.4	114.5	28.4	150.5	156.4	29.1
40/10/0.5	31.3	59.0	119.7	16.4	152.5	156.5	19.6
40/10/1	-	59.1	130.1	10.5	-	154.6	14.9
40/10/2	-	60.0	135.2	14.7	-	154.3	19.5

Scheme 1

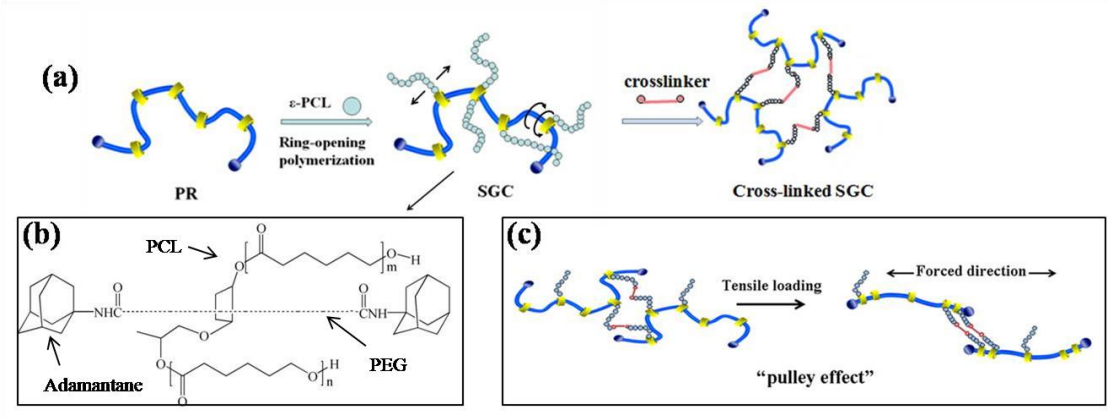

Scheme 1. (a) Schematic illustration of the preparation of a sliding graft copolymer (SGC), (b) structure schematic of SGC, (c) pulley effect.

Scheme 2

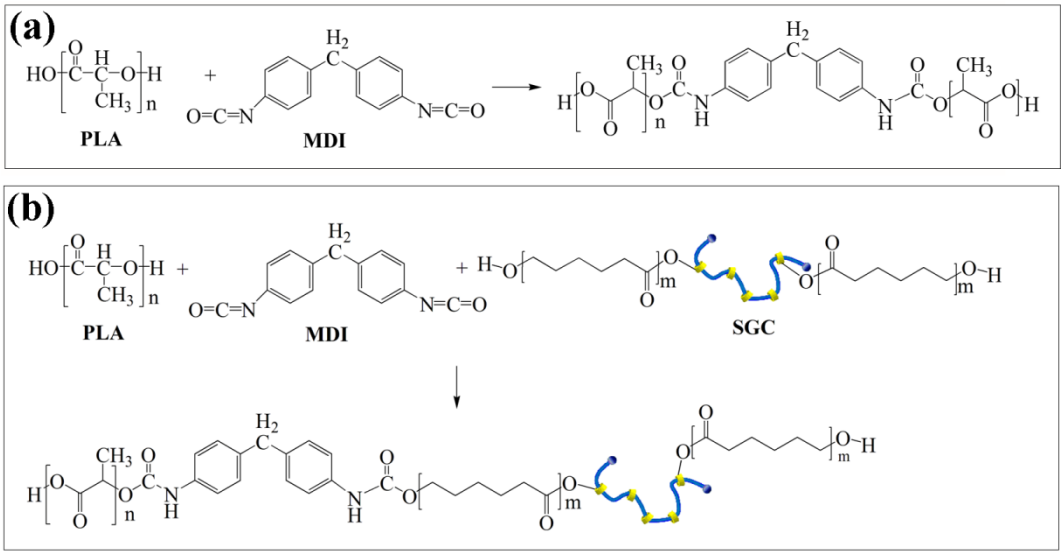

Scheme 2. Synthesis scheme of (a) chain extension of PLA with MDI, (b) compatibilizer PLA-*co*-SGC.

Figure 1

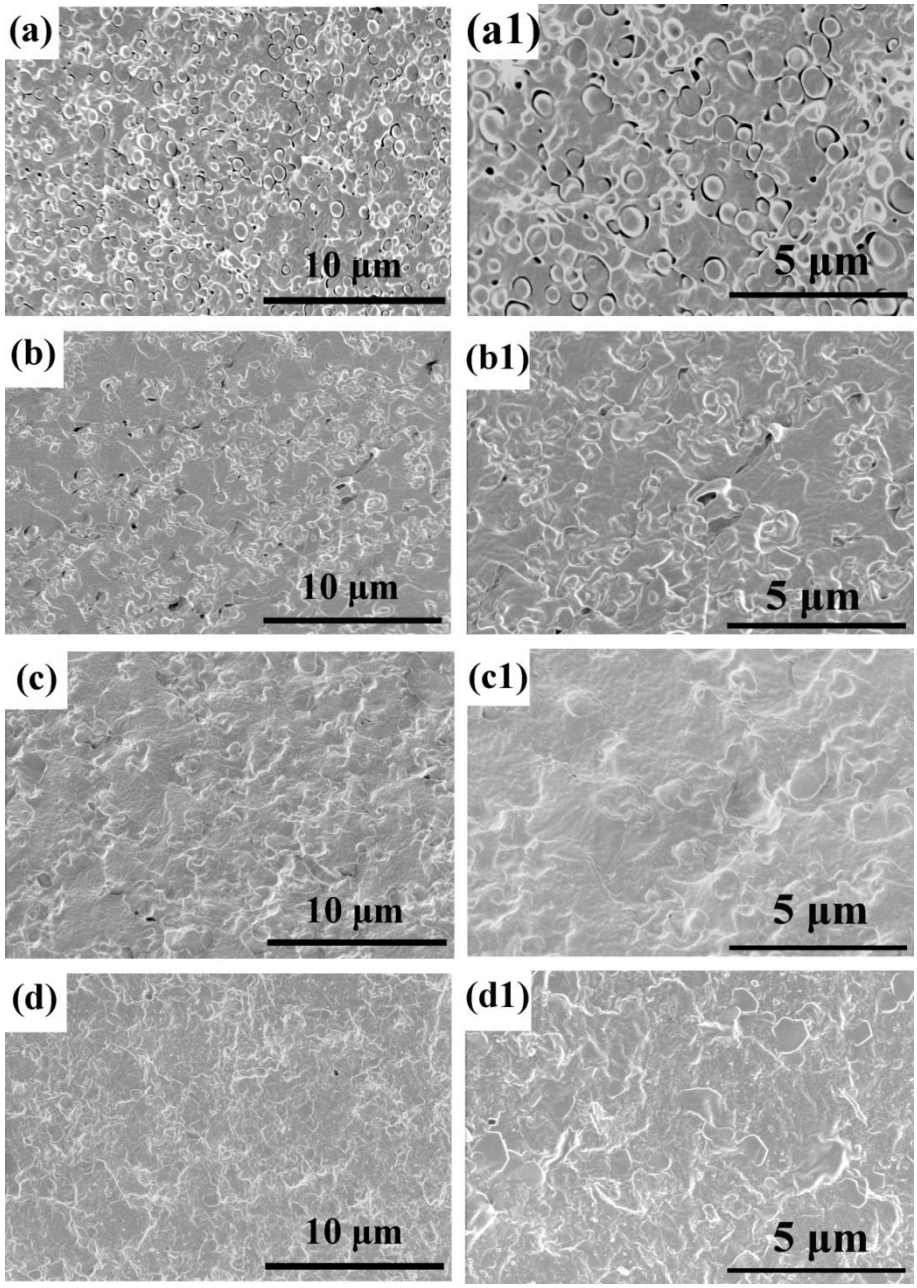

Figure 1. SEM images of cryo-fractured surface of PLA/SGC/MDI blends (a)-(a1) 40/10/0, (b)-(b1) 40/10/0.5, (c)-(c1) 40/10/1, (d)-(d1) 40/10/2

Figure 2

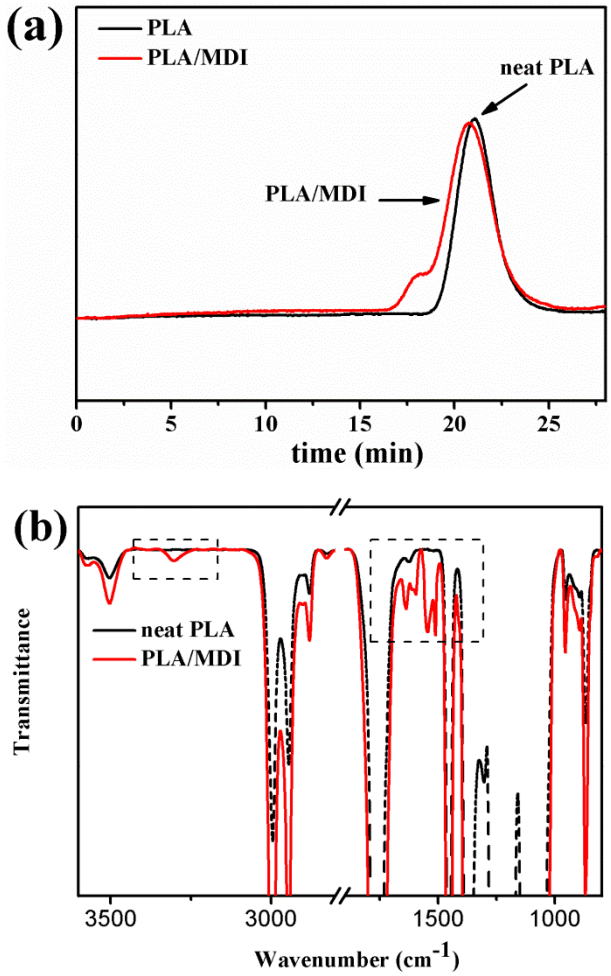

Figure 2. (a) GPC traces and (b) FTIR spectra of neat PLA and PLA/MDI (50/2) blend.

Figure 3

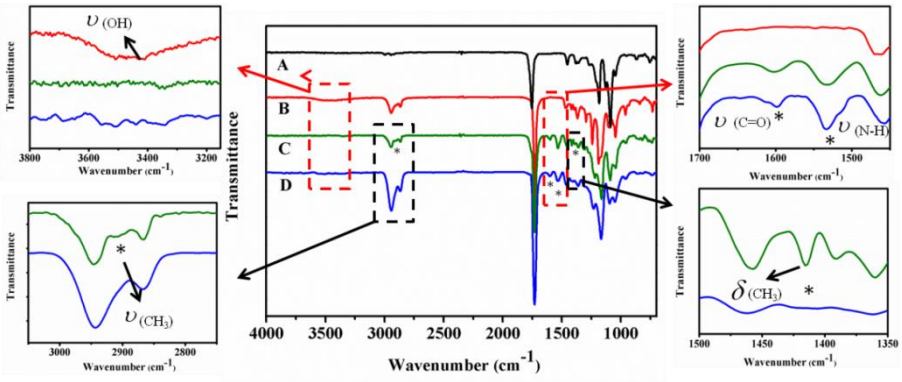

Figure 3. FTIR spectra of (A) neat PLA; (B) pure SGC; (C) c-SGC particles (extracted); (D) c-SGC particles (formed in flask)

Figure 4

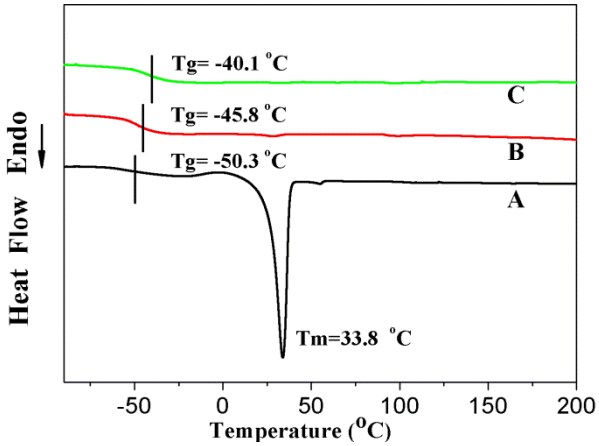

Figure 4. DSC curves of (A) pure SGC; (B) c-SGC particles (formed in flask); (C) c-SGC particles (extracted).

Figure 5

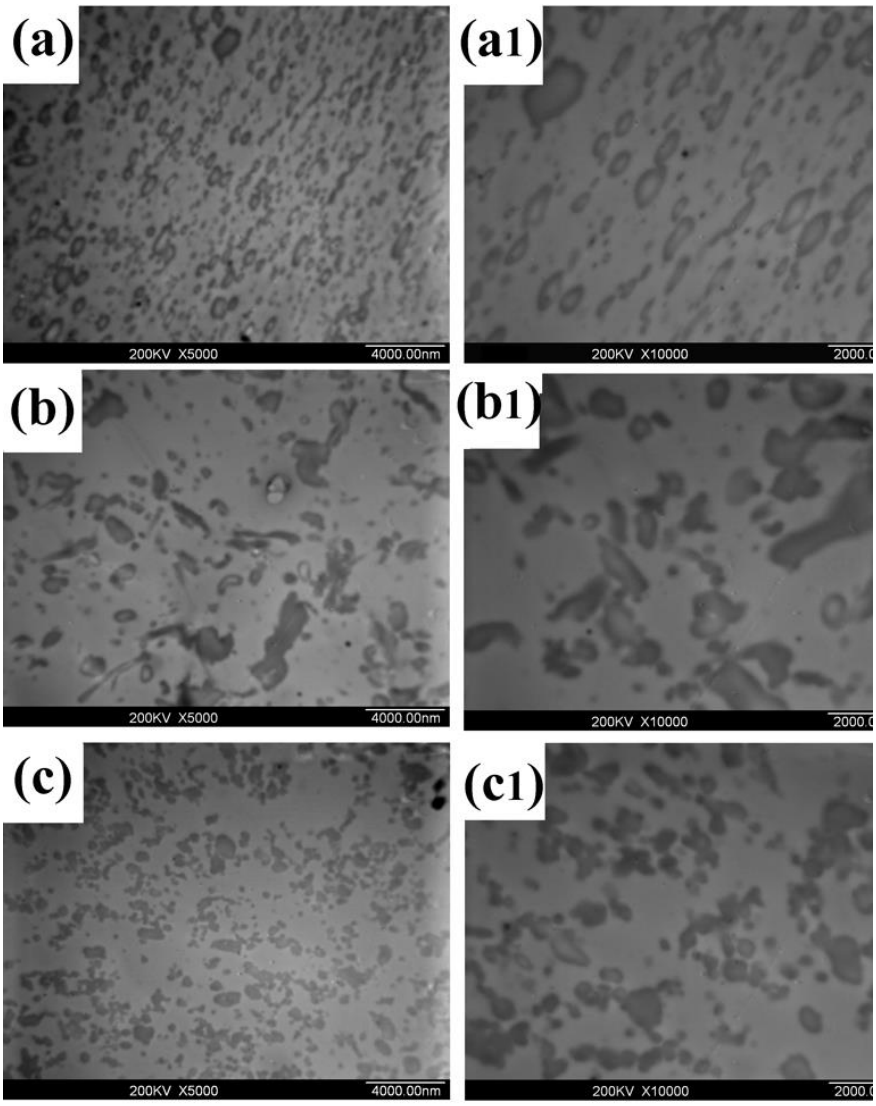

Figure 5. Transmission electron micrographs of (a)-(a1) PLA/SGC (40/10), (b)-(b1) PLA/ SGC/MDI (40/10/0.5), (c)-(c1) PLA/ SGC/MDI (40/10/2).

Figure 6

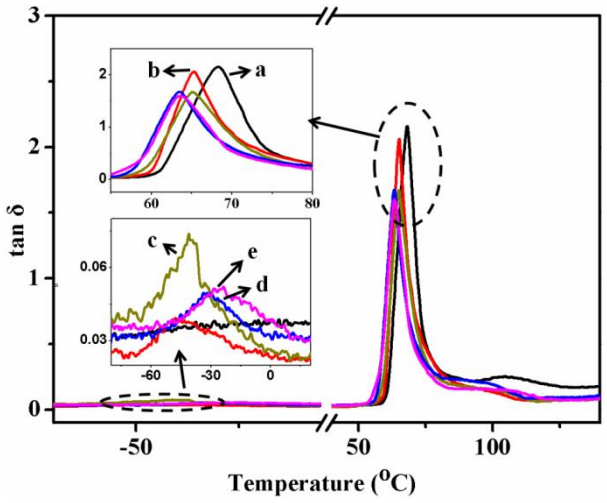

Figure 6. Plots of loss factor (tan δ) against temperature for (a) neat PLA, (b) PLA/SGC (40/10), (c) PLA/SGC/MDI (40/10/0.5), (d) PLA/SGC/MDI (40/10/1), and (e) PLA/SGC/MDI (40/10/2).

Figure 7

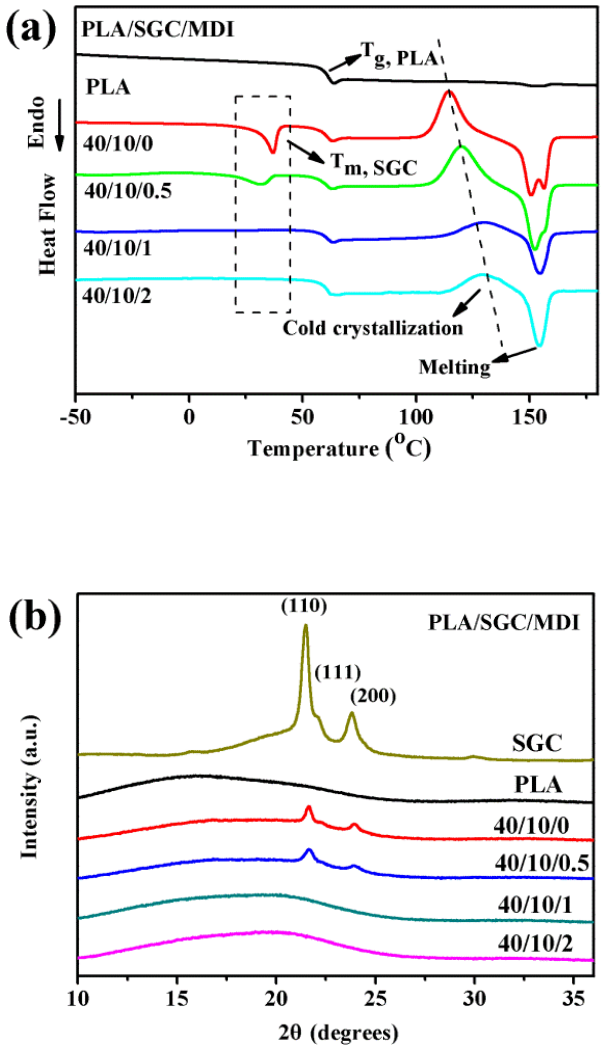

Figure 7. (a) DSC thermograms (second heating) and (b) XRD patterns of neat PLA, pure SGC, PLA/SGC, and PLA/SGC/MDI with different MDI amounts.

Figure 8

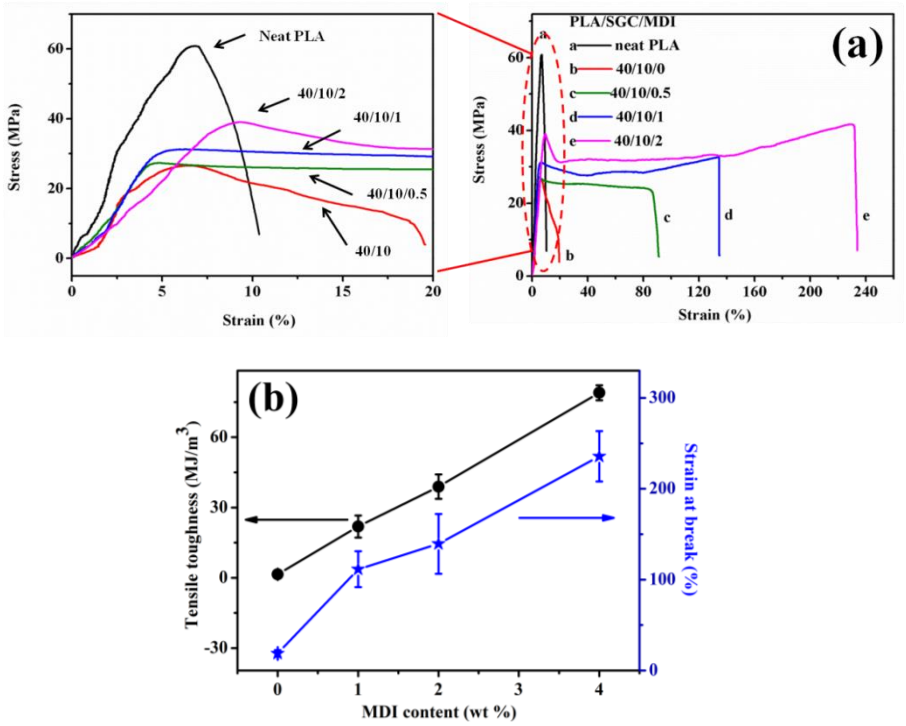

Figure 8. (a) Stress- strain curves and (b) tensile toughness and strain at break of PLA/SGC and PLA/SGC/MDI with different MDI contents.

Figure 9

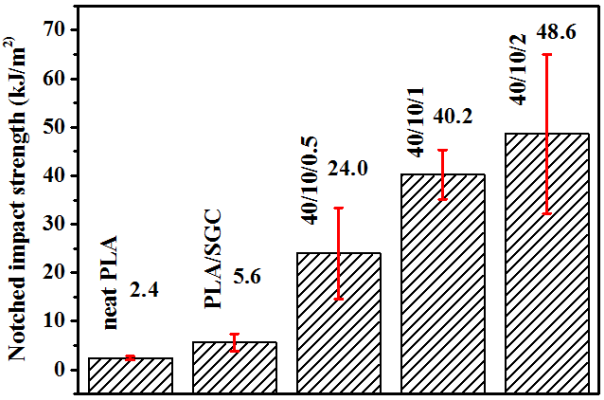

Figure 9. Notched impact strength of neat PLA, PLA/SGC, and PLA/SGC/MDI with different MDI contents.

Figure 10

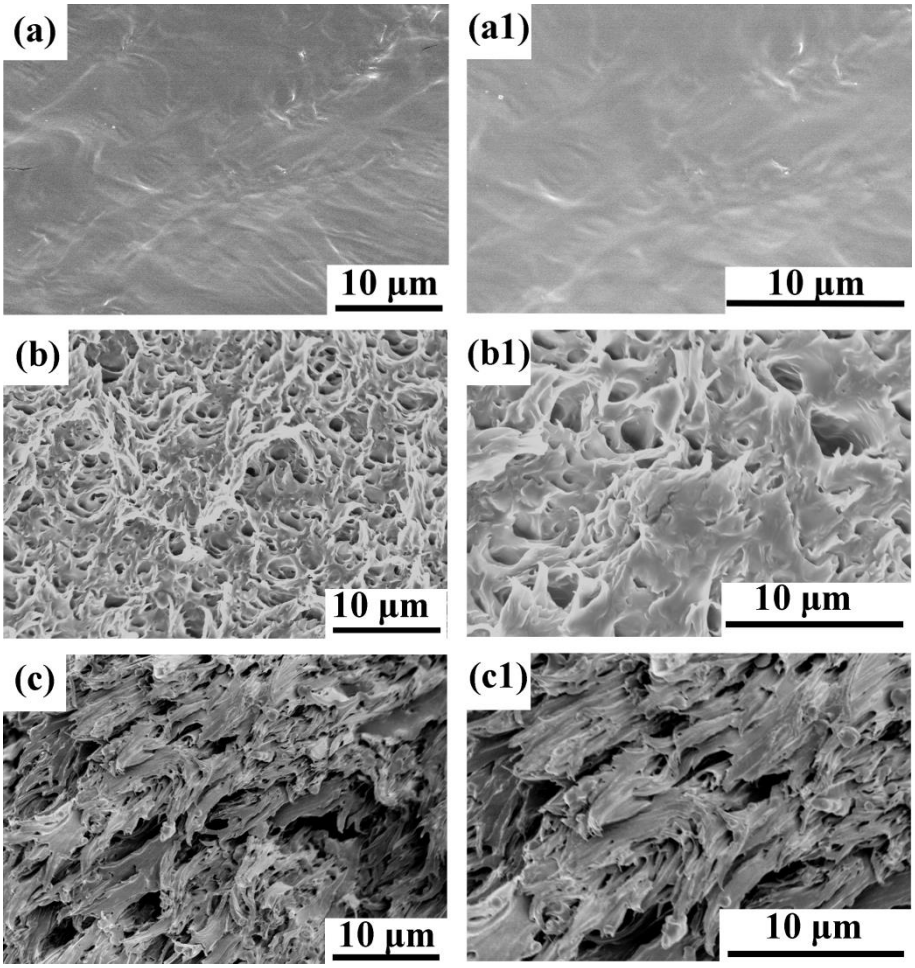

Figure 10. SEM images of tensile-fractured surface of (a)-(a1) neat PLA, (b)-(b1) PLA/SGC (40/10) and (c)-(c1) PLA/SGC/MDI (40/10/2)

Figure 11

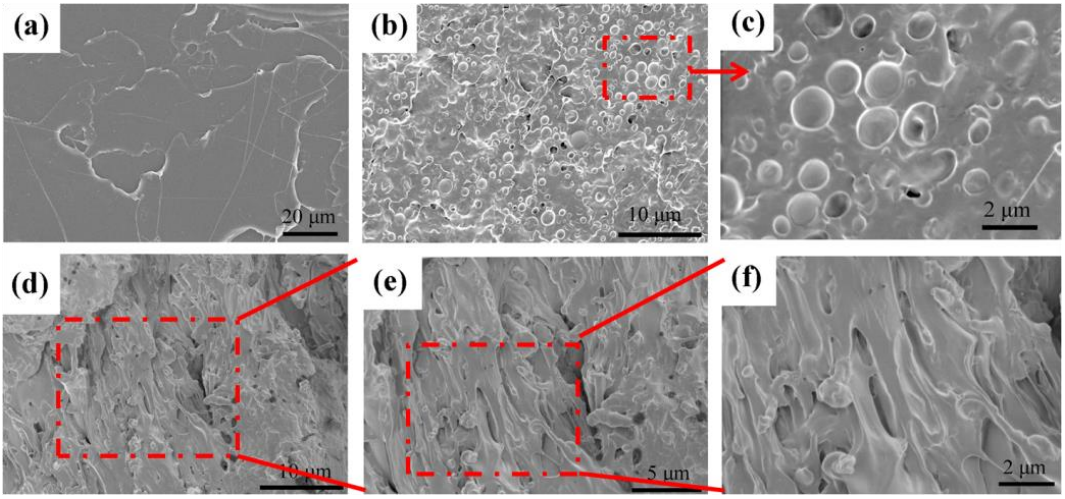

Figure 11. SEM images of impact-fractured surface of (a) neat PLA, (b)-(c) PLA/SGC (40/10), and (d)-(f) PLA/SGC/MDI (40/10/2).

Supplementary data

Highly Toughened Polylactide with Novel Sliding Graft Copolymer by in Situ Reactive Compatibilization, Crosslinking and Chain Extension

Xue Li [a], Hailan Kang [a], Jianxiang Shen [a], Liqun Zhang [a, b *], Toshio Nishi [c], Kohzo Ito [d *], Changming Zhao [d] and Phil Coates [e]

[a] State Key Laboratory for Organic-Inorganic Composites, Beijing University of Chemical Technology, Beijing 100029, China

[b] Key Laboratory of Beijing City for Preparation and Processing of Novel Polymer Materials, Beijing University of Chemical Technology, Beijing 100029, China

[c] Department of Applied Physics, The University of Tokyo, Hongo, Bunkyo-ku, Tokyo 113, Japan

[d] Department of Advanced Materials Science, Graduate School of Frontier Sciences, The University of Tokyo, 5-1-5 Kashiwanoha, Kashiwa, Chiba 277-8561, Japan

[e] School of Engineering, Design and Technology, Bradford University, Bradford, BD7 1DP, UK

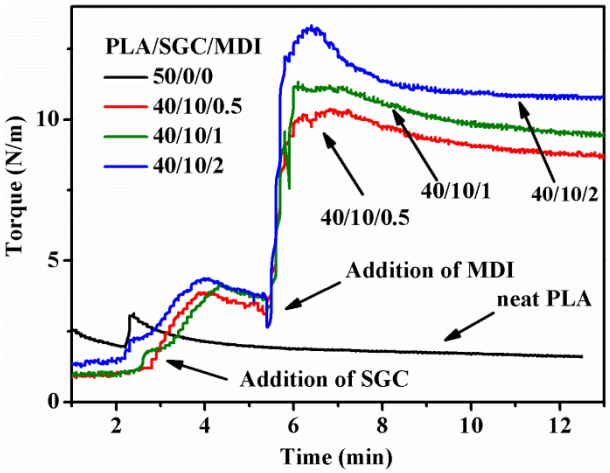

Figure S1. The effect of addition of methylene diphenyl diisocyanate (MDI) on the torque-time plot.

Figure S1 shows the tracking of torque during the mixing process for the neat PLA, and PLA/SGC/MDI blend with different amounts of MDI. As opposed to the torque of the neat PLA, which continuously decreases with time, the torque of PLA/SGC/MDI blends rises rapidly after the addition of MDI. This is attributed to the increased viscosity due to chemical reaction occurring between SGC, and some degree of PLA and SGC, as initiated by MDI and the hydroxyl end groups in the two polymer. The increase in the viscosity of blend could contribute to morphology modification by avoiding SGC's coalescence.

Table S1. Mechanical properties of PLA/SGC/MDI blends.

PLA/SGC/MDI (wt %)	TS (Mpa)	ε (%)	IS
50/0/0	60.8	13	2.4 [b1] 19.4 [b2]
40/10/0	26.3	19	5.2 [b1] 41.6 [b2]
40/10/0.5	27.3	112	22.0 [b1] 182.6 [b2]
40/10/1	30.6	134	40.9 [b1] 339.5 [b2]
40/10/2	41.7	236	48.6 [b1] 403.1 [b2]

Table S2. Summary of some previous effort for toughening PLA via blending toughener

Sample	Content (wt %)	TS (Mpa)	ε (Gpa)	IS	Ref
PLA/PBS/DCP	100/0/0	69.3± 0.9	4 ± 0.4	2.5±0.5 [b1]	[1]
	80/20/0	56.4 ± 1.0	250 ± 40	3.7± 0.3 [b1]	
	80/20/0.1	49.3 ± 0.9	249 ± 40	30.0±2.7 [b1]	
PLA/PCL/DCP	100/0/0	70 [a]	12 [a]	2 [a, b1]	[2]
	70/30/0	57 [a]	25 [a]	3.5 [a, b1]	
	70/30/0.3	48 [a]	130 [a]	4.9 [a, b1]	
PLA/PCL/LTI	100/0/0	-	-	-	[3]
	80/20/0	55.4 [b1]	22 [b1]	2.0 [b1]	
	80/20/0.5	47.3 [b1]	268 [b1]	17.3 [b1]	
PLA/PCL/TPA-100	80/20/0.5	-	-	58 [c]	[4]
PLA/PCL/24A-100	80/20/0.5	-	-	30 [c]	
PLA/PBSA/TPP	100/0/0	105[d]	6.4 [d]	6.76 [b1]	
	70/30/0	80 [d]	19.7 [d]	8.21 [b1]	
	70/30/2	60 [d]	19 [d]	11.4 [b1]	
	90/10/2	70 [d]	215 [d]	16.4 [b1]	
PLA/PBAT/T-GMA	100/0/0	-	-	-	[5]
	70/30/0	31 [a]	55 [a]	16 [a, b1]	
	70/30/2	27 [a]	180 [a]	32 [a, b]	
PLLA/ABS/SANMGA/ETPB	100/0/0/0	65.5	4.0	69.7 [c]	[6]
	50/50/0/0	33.8	3.5	48.3 [c]	
	50/50/5/0.02	43.6	23.5	162.8 [c]	
PLA/HBP/PA	100/0/0	76.5± 1.45	5.1 ± 1.7	2.6 ± 0.9 [d]	[7]
	92/08/0	64.2 ± 0.8	5.1 ± 1.0	1.6 ± 0.7 [d]	
	92/5.4/2.6	63.9 ± 1.7	48.3 ± 6.3	17.4 ± 1.5 [d]	
PLLA/LDPE/PE-b-PLLA	100/0/0	69.7	4.1	22 [b2]	[8]
	80/20/0	33.5	10.4	10.4 [b2]	
	80/20/10	31.4	35.3	283 [b2]	
PLLA/ABS/SANMGA/ETPB	100/0/0/0	65.5	4.0	69.7 [c]	[9]
	50/50	38.8	3.5	48.3[c]	
	50/50/5/0.02	43.6	23.5	162.8 [c]	
PC/PLA/ SAN-g-MAH	100/0/0	69	-	2.3[a, b1, e]	[10]
	70/30	56	-	22 [a, b, e]	
	70/30/5	66	-	37 [a, b, e]	
PLA/SEBS/EGMA	100/0/0	-	3	3 [b1]	[11]
	70/30	-	178	16 [b1]	
	70/20/10	-	185	92 [b1]	
PLA/TPU	100/0	67	4	4 [b1]	[12]

	70/30	35	600	40 [b1]	
PLA/PDLLA-PEG750	100/0	52	6	2.6 [b1]	[13]
	80/20	25	220	8.3 [b1]	
PLA/PEU	100/0	68	7.2	1.7 [b1]	[14]
PLA/LLDPE/PLLA-PE	100/0/0	-	-	20 [b2]	[15]
	80/20/5	24.3	31	660 [b2]	
PLA/EBA-GMA/EMAA-Zn	100/0/0	-	-	24.6 [b2]	[16]
	80/20/0	-	-	101.9 [b2]	
	80/20/5	-	-	859.8 [b2]	
PLA/EGMA	100/0	64.3	5	4 [a, b1]	[17]
	80/20	40	>200	70 [a, b1]	
PLLA/PE/ PLLA-PE	100/0/0	62.1	4	20 [b2]	[18]
	80/20/0	21.9	23	490 [b2]	

TS: Tensile strength; ε: Tensile elongation at break; IS: Impact strength.

[a] Estimated from graphical data in cited reference, since tabular was not provided.

[b1] Notched impact strength (kJ/m^2)

[b2] Notched impact strength (J/m)

[c] Unnotched impact strength

[d] Calculated as the area under stress-strain (MJ/m^2)

[e] converted Kg_f/cm^2 to MPa and kJ/m^2

Notched Izod impact strength of PLA/SGC/MDI (40/10/2) blend increases to 48.6 kJ/m^2, 20 times as compared to unmodified PLA, which is much higher than those reported in most literatures (table S2).

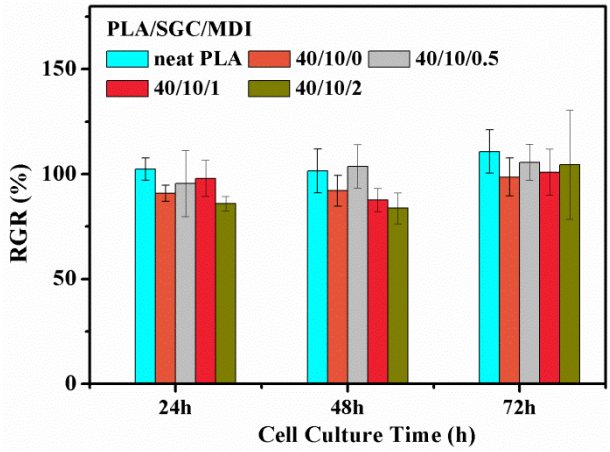

Figure. S2. Viability of L929 mouse fibroblasts as a function of incubation time. The bars represent standard deviation of three replicates

Table S3. The standard of the response grades

Grades	0	1	2	3	4	5
RGR	≥100	75-99	50-74	25-49	1-25	0

The cytotoxicity of neat PLA and PLA/SGC/MDI blends was evaluated to determine whether they are suitable for biomedical applications. L929 mouse fibroblasts were used in our cytotoxicity assays owing to their popularity and three days was chosen as the incubation period to allow for the completion at least one cell cycle. The cell relative growth rate (RGR) reflects the viability of L929 cells growing in the material. The RGR was classified to six grades as shown in Table S3 according to the standard GB/T 16886.5-2003. Grades 0 and 1 were accepted as qualified. Grade 2 should be considered by combining with the cell's morphology. Greater than grade 3 was considered as unqualified. A material would be considered as nontoxic when its RGR is at least 75 % higher than the control. In Figure S2, the RGR for neat PLA and PLA/SGC/MDI blends were are higher than 85 %, showing that PLA/SGC/MDI

blends have acceptable biocompatibility and hold great potential for both engineering and biomedical applications.

References

1. Wang, R.; Wang, S.; Zhang, Y.; Wan, C.; Ma, P. *Polymer Engineering & Science* **2009,** 49, (1), 26-33.
2. Semba, T.; Kitagawa, K.; Ishiaku, U. S.; Hamada, H. *Journal of Applied Polymer Science* **2006,** 101, (3), 1816-1825.
3. Harada, M.; Iida, K.; Okamoto, K.; Hayashi, H.; Hirano, K. *Polymer Engineering & Science* **2008,** 48, (7), 1359-1368.
4. Ojijo, V.; Sinha Ray, S.; Sadiku, R. *ACS Applied Materials & Interfaces* **2013,** 5, (10), 4266-4276.
5. Zhang, N.; Wang, Q.; Ren, J.; Wang, L. *J Mater Sci* **2009,** 44, (1), 250-256.
6. Al-Itry, R.; Lamnawar, K.; Maazouz, A. *Polymer Degradation and Stability* **2012,** 97, (10), 1898-1914.
7. Bhardwaj, R.; Mohanty, A. K. *Biomacromolecules* **2007,** 8, (8), 2476-2484.
8. Wang, Y.; Hillmyer, M. A. *Journal of Polymer Science Part A: Polymer Chemistry* **2001,** 39, (16), 2755-2766.
9. Li, Y.; Shimizu, H. *European Polymer Journal* **2009,** 45, (3), 738-746.
10. Lee, J. B.; Lee, Y. K.; Choi, G. D.; Na, S. W.; Park, T. S.; Kim, W. N. *Polymer Degradation and Stability* **2011,** 96, (4), 553-560.
11. Hashima, K.; Nishitsuji, S.; Inoue, T. *Polymer* **2010,** 51, (17), 3934-3939.
12. Han, J.-J.; Huang, H.-X. *Journal of Applied Polymer Science* **2011,** 120, (6), 3217-3223.
13. Lemmouchi, Y.; Murariu, M.; Santos, A. M. D.; Amass, A. J.; Schacht, E.; Dubois, P. *European Polymer Journal* **2009,** 45, (10), 2839-2848.
14. Jian Bing Zeng, Y.-D. L., Yi Song He, Shao Long Li, Yu Zhong Wang, In *10*, 2011; Vol. 50, pp 6124-6131.
15. Anderson, K. S.; Lim, S. H.; Hillmyer, M. A. *Journal of Applied Polymer Science* **2003,** 89, (14), 3757-3768.
16. Liu, H.; Song, W.; Chen, F.; Guo, L.; Zhang, J. *Macromolecules* **2011,** 44, (6), 1513-1522.
17. Oyama, H. T. *Polymer* **2009,** 50, (3), 747-751.
18. Anderson, K. S.; Hillmyer, M. A. *Polymer* **2004,** 45, (26), 8809-8823.